

Energetics of Cytoskeletal Gel Contraction

Matteo Ferraresso^{1,2}, Albert Kong^{1,2}, Mehadi Hasan^{1,2}, Gwynn J. Elfring¹, Daniele Agostinelli^{1,2},
Mattia Bacca^{1,2,*}

¹Mechanical Engineering Department, Institute of Applied Mathematics

²School of Biomedical Engineering

University of British Columbia, Vancouver BC V6T 1Z4, Canada

*Corresponding author: mbacca@mech.ubc.ca

Abstract

Cytoskeletal gels are prototyped to reproduce the mechanical contraction of the cytoskeleton in vitro. They are composed of a polymer network (backbone), swollen by the presence of a liquid solvent, and active molecules (molecular motors, MMs) that transduce chemical energy into the mechanical work of contraction. These motors attach to the polymer chains to shorten them and/or act as dynamic crosslinks, thereby constraining the thermal fluctuation of the chains. We describe both mechanisms thermodynamically as a microstructural reconfiguration, where the backbone stiffens to motivate solvent (out)flow and accommodate contraction. Via simple steady state energetic analysis, under the simplest case of isotropic contraction, we quantify the mechanical energy required to achieve contraction as a function of polymer chain density and molecular motor density. We identify two limit cases, (*fm*) fast MM activation for which MMs provide all the available mechanical energy ‘instantaneously’ and leave the polymer in a *stiffened* state, *i.e.* their activity occurs at a time scale that is much smaller than solvent diffusion, and (*sm*) slow MM activation for which the MM activation timescale is much longer. To achieve the same final contracted state, *fm* requires the largest amount of work per unit reference volume, while *sm* requires the least. For all intermediate cases where the timescale of MM activation is comparable with that of solvent flow, the required work ranges between the two cases. We provide all these quantities as a function of chain density and MM density. Finally, we compare our results with experiments and observe good agreement.

Keywords: Active soft matter; polymer gels; cytoskeleton; contraction; energetics

Introduction

The cytoskeleton is the structural backbone of the cell and is primarily made up of actin, intermediate filaments and microtubules [1]. Actin filaments coupled with myosin motors actively partake in the mechanical response of the cell and are responsible for its contractile behaviour. Actomyosin II complexes pull on the actin chains to shorten them, therefore the 3D meshwork of crosslinked actin chains contracts. This process is mainly powered by adenosine triphosphate (ATP) hydrolysis, where released chemical energy from the breakdown of ATP into ADP and a phosphate, is expended in the form of mechanical work. This is a critical function required for motility, environmental adaptation, chemical transport, and intracellular signaling [1]. Understanding cytoskeletal contraction from mechanical and energetic standpoints is critical to characterize tissue properties and tissue mechanics.

Cytoskeletal gels are engineered to mechanically model the cytoskeleton. They constitute a minimalistic physical system by including only the main components of the cytoskeleton: polymer chains and cytoplasm; while excluding organelles, membranes and other cell components [2,3]. Figure 1 outlines the main components of the gel and their arrangement in the system. These gels have been used to both characterize the mechanical properties of the cytoskeleton and to study cell contractility.

The first theoretical models formulated to describe cytoskeletal contraction approached the problem from a hydrodynamic standpoint, where transient force dipoles, generated by myosin pulling on actin chains, create active contractile stresses [4,5]. The main limitation of such models lies in their assumption that actin filaments must not be slack, and this is not the case for some actin networks [5]. Furthermore, these models describe active stresses using parameters that are empirically determined, and typically lack physical meaning. Gels composed of slack chains are not well represented by these models as the cytoskeletal active stresses do not account for the level of tension in the chains. To overcome this limitation, recent studies propose an alternative approach based on poroelasticity, where the cytoskeleton is described as a polymer network swollen by the presence of the solvent (cytosol) [6]. In this biphasic material, the passive behavior is controlled by swelling and solvent flow [7,5,8, 9, 10,11], while the active behavior is described as an evolution of the mechanical stiffness of the polymer backbone [7] and is promoted by molecular motor activity. The total free energy of the gel is given by the sum of the strain energy of the network and the free energy (enthalpy and entropy) of chain-solvent mixing. The activation of contractile molecular motors (MM) increases the strain energy, representing a stiffening of the chain network [7,2,12,13,14]. This in turn increases the osmotic pressure of the solvent, locally, and, with it, the chemical potential of the solvent. Because the flow of the solvent is directed toward a reduction in chemical potential, via Fick's law, the solvent ultimately outflows the stiffened gel, thereby accommodating gel contraction [7,15,16]. Polymer network stiffening can be achieved via dynamic crosslinking (DC) created by a MM attaching to more than one chain. This is described in some models as an evolution of the crosslink density [7,15].

The observed MM activity in actin cytoskeletal gels primarily involves chain shortening (CS) rather than DC [2]. Figure 1 presents the two motor activation mechanisms. An energetically based model incorporating realistic MM activation applicable to in-vivo environments is therefore necessary to fully understand actin gel contractile mechanics. This study builds on active polymer gel theory and introduces a new molecular motor model considering chain shortening (CS), striving towards a more accurate representation of the physical system. Our model introduces a new thermodynamically inspired variation of neo-Hookean chain strain energy to incorporate a CS parameter we define as the 'microstretch'. This parameter decouples chain density from contractile mechanics, allowing for direct comparison between the energetic requirement for a specific contraction (quantity of molecular motors) and initial chain density. Experiments using an in-vitro actin network platform reveal a threshold for the minimum quantity of MM required to achieve a desired contraction [17,18]. Via quasi-static energetic analysis, we use our model to predict this threshold in a direct comparison with experimental data of contractile acto-myosin networks. Moreover, we compute a maximum MM density, for a given crosslink density, above which contraction is also prevented due to motor-chain detachment [19,20].

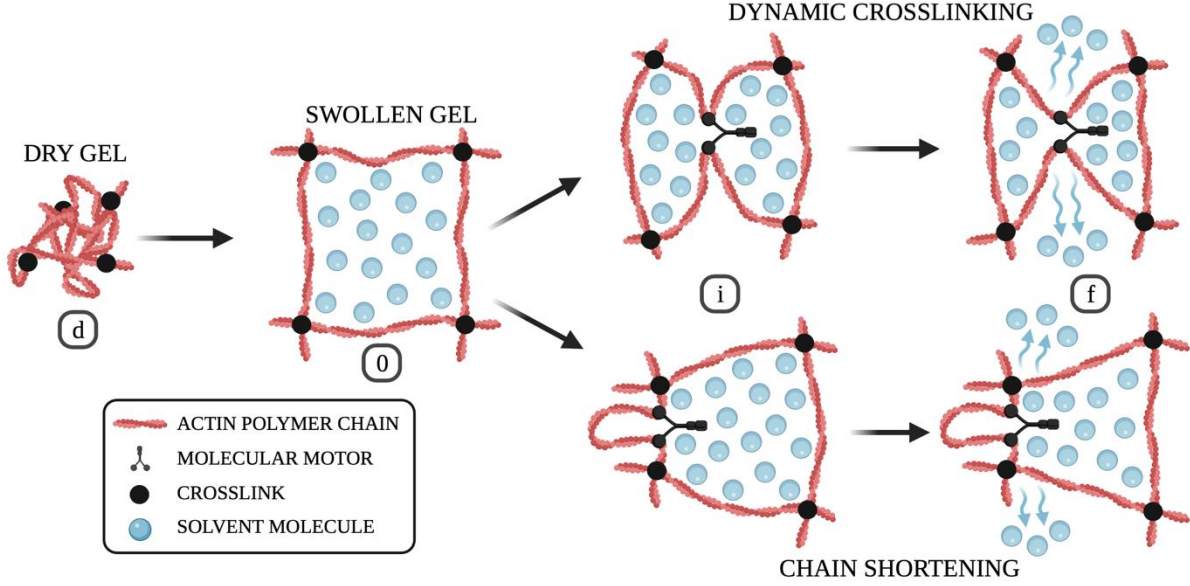


Figure 1 – Diagram outlining the two main mechanisms of cytoskeletal gel contraction: dynamic crosslinking (DC, top) and chain shortening (CS, bottom). The gel is initially in its reference dry configuration (d). It is then swollen by solvent (blue spheres) and in equilibrium with the environment (0). When activated, the motors inject energy by stiffening the polymer backbone (i), which causes solvent outflow accommodating contraction (f). DC motors attach to different chains in the network, thereby increasing the crosslink density. CS motors decrease the average chain length.

Active Gel Model

The biphasic active gel is composed of a (swollen) polymer network, a solvent, and molecular motors (Fig. 1). The polymer chains provide the structural backbone of the gel, and are stretched to accommodate the presence of the solvent. We define the dry polymer network (prior to solvent absorption and swelling) as the stress-free reference state of the gel (albeit for some gels this is an idealized state since the polymer dissociates in the absence of solvent).

The total free energy density, per unit *reference volume* V_d , as described by [7], is

$$\psi = \psi_e(T, \mathbf{F}, \boldsymbol{\zeta}) + \psi_m(T, C) + \Pi(1 + \Omega C - J) \quad (1)$$

where ψ_e is the elastic strain energy density of the polymer network, ψ_m is the free energy density of polymer-solvent mixing, Π is the hydrostatic pressure applied to the gel, C is the molecular concentration of solvent, per unit reference volume, Ω is the molecular volume of the solvent and J is the swelling ratio of the gel (current volume to reference volume). In Eq. (1), T is the absolute temperature, \mathbf{F} is the deformation tensor defined as

$$F_{jk} = \frac{\partial x_j}{\partial X_k} \quad (2)$$

With \mathbf{x} the position of the material points in the current state and \mathbf{X} that in the reference state, $\boldsymbol{\zeta}$ is the vector of microstructural parameters describing the elastic response of the polymer network. Π serves as a Lagrange multiplier to enforce molecular incompressibility of the solvent so that

$$J = 1 + \Omega C \quad (3)$$

Considering the solvent bath is isothermal, from the first and second laws of thermodynamics [7] (see Appendix A), we obtain

$$t_{jk} = \frac{\partial \psi}{\partial F_{jk}} \quad (4)$$

$$\mu = \frac{\partial \psi}{\partial C} \quad (5)$$

and

$$dw_l = \frac{\partial \psi}{\partial \zeta_l} d\zeta_l \quad (6)$$

where \mathbf{t} is the first Piola-Kirchoff stress tensor, μ is the chemical potential of the solvent, dw_l is the unit work, per unit reference volume, provided by the MM to produce a unit change $d\zeta_l$ for the microstructural variable ζ_l .

To ensure mechanical equilibrium, we need

$$\frac{\partial t_{jk}}{\partial X_k} + B_j = 0 \text{ in } V_d \quad (7a)$$

and

$$t_{jk} N_k = T_j \text{ on } S_d \quad (7b)$$

with \mathbf{B} the body force vector, \mathbf{N} the unit outward normal to S_d , *i.e.* the boundary of V_d , and \mathbf{T} the external traction force. \mathbf{B} is a force per unit V_d , while \mathbf{T} is a force per unit S_d .

Assuming the gel boundary S_d is permeable, a free exchange of solvent molecules with the external bath imposes

$$\mu = \mu_{ext} \text{ on } S_d \quad (8a)$$

with μ_{ext} the chemical potential of the solvent in the bath. Conversely, in the case of impermeable boundary, one should instead impose

$$H_i N_i = 0 \text{ on } S_d \quad (8b)$$

(with repeated indices indicating the sum) with \mathbf{H} the solvent flux given by Fick's law [6].

At chemical equilibrium, assuming at least a portion of S_d is permeable, we have

$$\mu = \mu_{ext} \text{ in } V_d \quad (9)$$

Mixing free energy

Assuming the polymer network is dilute into the solvent, *i.e.* $J \gg 1$, ψ_m can be described with the bimolecular mixing free energy theory introduced by [21] and giving

$$\frac{\psi_m}{kT} = C \left[\ln \left(\frac{\Omega C}{1 + \Omega C} \right) + \frac{\chi}{1 + \Omega C} \right] \quad (10)$$

where k is the Boltzmann constant. The first term on the right-hand side of Eq. (10) provides the entropic contribution, and is based on the *liquid lattice* theory. The second term describes the

enthalpy of mixing, where χ is the mixing-enthalpy parameter and $\chi > 0$ describes the steric repulsions between solvent and polymer, thereby favoring un-mixing [21].

Elastic free energy

We assume the polymer backbone is described by a network of Gaussian chains with variable length, yielding the modified neo-Hookean elastic free energy density (see Appendix B)

$$\frac{\psi_e}{kT} = \frac{N}{2} \left[\frac{F_{jk}F_{jk}}{\lambda_m^2} - 2 \ln \left(\frac{J}{\lambda_m^3} \right) - 3 \right] \quad (11)$$

Here, N is the chain density in the unit reference volume, and $\lambda_m = m/m_0$ is the chain microstretch parameter, with m the average number of free monomers between crosslinks of the contracted chain, and m_0 the original one. In the case of $\lambda_m = 1$ no chain microstretch occurs and the strain energy expression becomes that of a swollen incompressible neo-Hookean. The microstructural variable ζ is therefore composed of N and λ_m , where DC MM's are associated with an evolution of N , while CS MM's are associated with an evolution of λ_m . We will analyze both mechanisms separately. Note that N is defined in the dry state ($N = N_d$). The resulting chain density in the current configuration is defined as $\hat{N} = N/J$.

Isotropic contraction of unloaded gels

Consider now an unloaded gel. By substituting Eq. (11) into (1), and the result into (4), because the Cauchy stress is $\sigma_{ij} = t_{ik}F_{jk}/J$, we obtain

$$\sigma_{jk} = \frac{NkT}{J} \left[\frac{F_{ji}F_{ki}}{\lambda_m^2} - \delta_{jk} \right] - \Pi \delta_{jk} \quad (12)$$

In the absence of body forces, we can assume the stress components are constant within the gel. Because the stress has to equilibrate the external pressure Π_{ext} applied to the gel from the environment (the solvent bath), we have that $\sigma_{jk} = -\Pi_{ext}\delta_{jk}$ for each j, k couple. By imposing this condition to Eq. (12), we must have $F_{ji}F_{ki} = \delta_{jk}$. This condition is satisfied in the case of isotropic swelling of the gel, where the deformation is characterized by equal principal stretches λ in all directions as function of the swelling ratio $J = \lambda^3$. Substituting this condition into Eq. (12) we have the hydrostatic gel pressure

$$\Pi = \Pi_{ext} + \Pi_{osm} \quad (13a)$$

with

$$\Pi_{osm} = \frac{NkT}{J} \left(\frac{J^{2/3}}{\lambda_m^2} - 1 \right) \quad (13b)$$

the osmotic pressure of the solvent. Π_{osm} is also the hydrostatic swelling stress that stretches the polymer chains to accommodate the presence of the solvent.

By substituting Eq. (10) into (1), and the result into (5), we obtain the chemical potential of the solvent as

$$\mu = kT \left[\ln \left(\frac{\Omega C}{1 + \Omega C} \right) + \frac{\chi + 1 + \Omega C}{(1 + \Omega C)^2} \right] + \Pi \Omega \quad (14)$$

Substituting Eq. (3) and (13) into (14) (see full derivation in Appendix C), we have

$$\bar{\mu} = \ln\left(1 - \frac{1}{J}\right) + \frac{\chi+J}{J^2} + n\left(\frac{1}{\lambda_m^2 J^{1/3}} - \frac{1}{J}\right) \quad (15a)$$

with

$$\bar{\mu} = \frac{\mu - \Omega \Pi_{ext}}{kT} \quad (15b)$$

the dimensionless net chemical potential, and $n = \Omega N$ the dimensionless crosslink density (*i.e.* the number of crosslinks per number of solvent molecules). At chemo-mechanical equilibrium we have $\bar{\mu} = \bar{\mu}_{ext}$, with $\bar{\mu}_{ext}$ obtained from Eq. (15b) by substituting μ with μ_{ext} .

From Eq. (15) we can obtain the derivatives of $\bar{\mu}$ with respect to the microstructural variables N and λ_m as

$$\frac{1}{\Omega} \frac{\partial \bar{\mu}}{\partial N} = \frac{1}{\lambda_m^2 J^{1/3}} - \frac{1}{J} \quad (16a)$$

$$\frac{1}{\Omega} \frac{\partial \bar{\mu}}{\partial \lambda_m} = -\frac{2N}{\lambda_m^3 J^{1/3}} \quad (16b)$$

Eq. (16) shows that polymer stiffening via increment of N (DC-MM) or reduction of λ_m (CS-MM) always produces an increment of μ . So if $\bar{\mu} = \bar{\mu}_{ext}$, before any MM activity, we will have $\bar{\mu} > \bar{\mu}_{ext}$ after MMs are activated. Because the solvent flux \mathbf{h} follows Fick's law [6]

$$h_i = -D \frac{C}{J} \frac{\partial \bar{\mu}}{\partial x_i} \quad (17)$$

i.e., the solvent migrates from high- $\bar{\mu}$ regions to low- $\bar{\mu}$ ones, the solvent will exit the gel to join the buffer (external solvent bath); this process reduces μ to recover chemical equilibrium. This occurs if

$$\frac{1}{\Omega} \frac{\partial \bar{\mu}}{\partial C} = \frac{1}{J^2(J-1)} - \frac{2\chi}{J^3} + n\left(\frac{1}{J^2} - \frac{1}{3J^{4/3}\lambda_m^2}\right) \quad (18)$$

is positive so that $\bar{\mu}$ decreases to $\bar{\mu}_{ext}$ while J decreases to its new equilibrium value. The positivity of the right-hand side of Eq. (18) depends on χ , N , λ_m and J , thus posing some physical constraints to contraction. The most limit physical constraint, however, is due to free energy reduction, for which

$$\frac{\partial \psi}{\partial J} J + \frac{\partial \psi}{\partial C} \dot{C} \leq 0 \quad (19)$$

where the equality applies for the case of quasi-static contraction. Substituting Eq. (3), (5) and (15) into (19), the latter gives the following condition

$$\bar{\mu} \dot{C} \leq 0 \quad (20)$$

In Eq. (20), contraction occurs if $\dot{C} < 0$, which is spontaneous if $\bar{\mu} \geq 0$. Conversely, swelling involves $\dot{C} > 0$, which is spontaneous if $\bar{\mu} \leq 0$. From these observations, one can deduce that the gel is in chemo-mechanical equilibrium, *i.e.* with no driving force for swelling nor contraction, when $\bar{\mu} = 0$. Since $\bar{\mu}$ is defined as

$$\bar{\mu} = \frac{1}{\Omega} \frac{d\bar{\psi}}{dC} \quad (21)$$

with $\bar{\psi} = \psi \Omega / kT$ the dimensionless free energy, $d(\bar{\psi})/dC = \partial(\bar{\psi}_e)/\partial C + \Omega \partial(\bar{\psi}_m)/\partial J$, and considering the condition of the positive derivative from Eq. (18), chemo-mechanical equilibrium,

(*i.e.* $\bar{\mu} = 0$), occurs at a free energy minimum. Because the chemo-mechanical equilibrium also imposes $\bar{\mu} = \bar{\mu}_{ext}$, one must conclude that $\bar{\mu}_{ext} = 0$. In the solvent bath, $\mu_{ext} = \Omega(P - P_0)$ [6], with P the solvent pressure and P_0 the vapor (cavitation) pressure. Taking $\Pi_{ext} = P - P_0$ as the relative pressure of the solvent bath, we finally have $\bar{\mu}_{ext} = 0$.

In the following derivation, we will compare the free energy at three states: (0) the swollen equilibrium state, prior to MM activation; (*i*) the initial state when MM are activated and provide all the available mechanical work to stiffen the backbone; (*f*) the final state at which all the contraction has occurred and the stiffened gel reached a new equilibrium configuration. The swelling ratio in (0) and (*i*) is the same, assuming MM activity is much faster than solvent diffusion. In this case $J = J_0$.

For the generic state $s = 0, i, f$, the dimensionless free energy can be rewritten from Eq. (1), (10) and (11) as

$$\bar{\psi}_s = \bar{\psi}_{e,s} + \bar{\psi}_{m,s} \quad (22a)$$

$$\bar{\psi}_{e,s} = n_s \left[\frac{3}{2} \left(\frac{J_s^{2/3}}{\lambda_{m,s}^2} - 1 \right) - \ln J_s \right] \quad (22b)$$

$$\bar{\psi}_{m,s} = (J_s - 1) \ln \left(1 - \frac{1}{J_s} \right) + \chi \left(1 - \frac{1}{J_s} \right) \quad (22c)$$

where $n_s = N_s \Omega$ is the dimensionless crosslink density, $\lambda_{m,s}$ the chain micro-stretch, and J_s the swelling ratio at state s .

At state (0), J_0 is determined from Eq. (15) at chemical equilibrium by imposing the condition $\bar{\mu} = 0$ in Eq. (15a), with $n = n_0$, $\lambda_m = 1$, and $J = J_0$.

To achieve contraction, the swelling ratio must reduce from (*i*) to (*f*), thus $J_f < J_i$. At (*i*), while $J_i = J_0$, the microstructure has evolved via increase in chain density, giving $n_i = N_i \Omega > n_0$ (DC), and/or shortening of chains, giving $\lambda_{m,i} < 1$ (CS). Both these mechanisms induce network stiffening, thereby increasing the osmotic pressure, which in its dimensionless form $\bar{\Pi}_{osm} = \Pi_{osm} \Omega / kT$, from Eq. (13b), becomes

$$\bar{\Pi}_{osm,i} = \frac{n_i}{J_0} \left(\frac{J_0^{2/3}}{\lambda_{m,i}^2} - 1 \right) \quad (23)$$

Now the free energy is given by Eq. (22) with $J_i = J_0$, $n = n_i$, and $\lambda_m = \lambda_{m,i}$. This gives $\bar{\psi}_{m,i} = \bar{\psi}_{m,0}$, while $\bar{\psi}_{e,i} > \bar{\psi}_{e,0}$, from which, $\bar{\psi}_i > \bar{\psi}_0$.

To define the state (*f*) we must impose again chemical equilibrium. This involves the condition $\bar{\mu} = 0$ in Eq. (15a) with $n = n_i$, $\lambda_m = \lambda_{m,i}$, and $J = J_f$. The free energy in this state is given again by Eq. (22) with J_f , $n_f = n_i$, and $\lambda_{m,f} = \lambda_{m,i}$.

The ratio J_f/J_0 defines the contraction obtained, which, intuitively, is proportional to the ratio n_i/n_0 and/or $1/\lambda_{m,i}$. However, as shown in the Results section, the contraction amount depends on the initial conditions defined by J_0 and n_0 .

Let us now introduce the microstructural mechanical work, w_m , per unit reference volume, with its dimensionless form $\bar{w}_m = w_m \Omega / kT$. We have then that the work due to *fast* MM activation, *i.e.* with sudden injection of all the microstructural work available, is

$$\bar{w}_{fm} = \bar{\psi}_i - \bar{\psi}_0 \quad (24)$$

In this case we assume that the time scale for MM activation is much shorter than that due to solvent flow. Also, we assume that after the MM perform all the microstructural work to stiffen the polymer, they stay in place and the polymer stays in its new stiffened state. That means that λ_m remains $\lambda_{m,f} = \lambda_{m,i}$, and n remains $n_i = n_f$.

In the case of *slow* MM activation, *i.e.* when the time scale for MM activation is much longer than that for solvent flow, we have that the work performed by the MM to achieve the final state is

$$\bar{w}_{sm} = \bar{\psi}_f - \bar{\psi}_0 \quad (25)$$

Because contraction is spontaneous, we will always have $\bar{\psi}_i \geq \bar{\psi}_f$, and thus $\bar{w}_{fm} \geq \bar{w}_{sm}$. Also, in intermediate cases for which the time scale for MM activation is comparable with that of solvent flow, we have that $\bar{w}_{sm} \leq \bar{w}_m \leq \bar{w}_{fm}$. This means that \bar{w}_{sm} is the minimum work required to reach the state f , while \bar{w}_{fm} is the maximum.

Results and discussion

As discussed in the previous section, chemo-mechanical equilibrium is obtained from the condition of homogeneous distribution of chemical potential, equal to that of the solvent bath, thus, $\bar{\mu} = 0$. From Eq. (15), this condition imposes

$$n = \frac{J \ln(1-1/J) + 1 + \chi/J}{1 - J^{2/3} \lambda_m^{-2}} \quad (26)$$

Figure 2-left reports the values of compatible J versus n for various values of χ and λ_m , from Eq. (26). Larger equilibrium swelling requires lower crosslink density, thus making J and n inversely proportional. The log-log plot in this figure shows a linear trend giving $n \sim \chi \lambda_m^2 J^{-3/5}$ for larger J and smaller χ . Taking $\lambda_m = 1$, this figure is useful to obtain J_0 from n_0 . In the case of DC-MM, the same figure with $\lambda_m = 1$ can also give J_f from n_f . The marker in this figure indicates the experimentally observed values of $J_0 = 1000$, $n_0 = 1.35 \cdot 10^{-6}$ and $\lambda_{m,0} = 1$, with $N_0 = 5.09 \cdot 10^{22} m^{-3}$, and $\Omega = 3 \cdot 10^{-30} m^3$, (see Appendix C for derivations), compatible with $\chi = 0.37$.

For all the datapoints in this figure, the positivity of

$$\frac{1}{\Omega} \frac{\partial \bar{\mu}}{\partial c} = \frac{1}{J^2(J-1)} - \frac{2\chi}{J^3} + \frac{J \ln(1-1/J) + 1 + \chi/J}{1 - J^{2/3} \lambda_m^{-2}} \left(\frac{1}{J^2} - \frac{1}{3J^{4/3} \lambda_m^2} \right) \quad (27)$$

from Eq. (18), is always satisfied. *I.e.* the chemo-mechanical equilibrium at $\bar{\mu} = 0$ is always stable.

By rearranging Eq. (26), one can also obtain

$$\lambda_m^2 = \frac{n J^{5/3}}{J(n-1) - \chi - J^2 \ln(1-1/J)} \quad (28)$$

Figure 2-right reports the values of compatible J versus λ_m^2 for various values of χ and n , from Eq. (28). Because smaller microstretch λ_m^2 give stiffer gels, and thus smaller equilibrium swelling J , λ_m^2 and J are proportional. The log-log plot in this figure shows a linear trend giving $\lambda_m^2 \sim -n J^{5/3} / \chi$ for larger J and smaller χ . In the case of CS-MM, this figure can be used to identify J_f from a given $n = n_0$ and λ_m^2 . In this figure, the marker highlights again the point at which $J_0 = 1000$, $n_0 = 1.35 \cdot 10^{-6}$, and $\lambda_{m,0}^2 = 1$. For all the datapoints in this figure, the positivity of

$$\frac{1}{\Omega} \frac{\partial \bar{\mu}}{\partial C} = \frac{2+J}{3J^2(J-1)} + \frac{2}{3} \frac{n}{J^2} - \frac{5}{3} \frac{\chi}{J^3} + \frac{1}{3J} \ln \left(1 - \frac{1}{J} \right) \quad (29)$$

from Eq. (18), is again always satisfied.

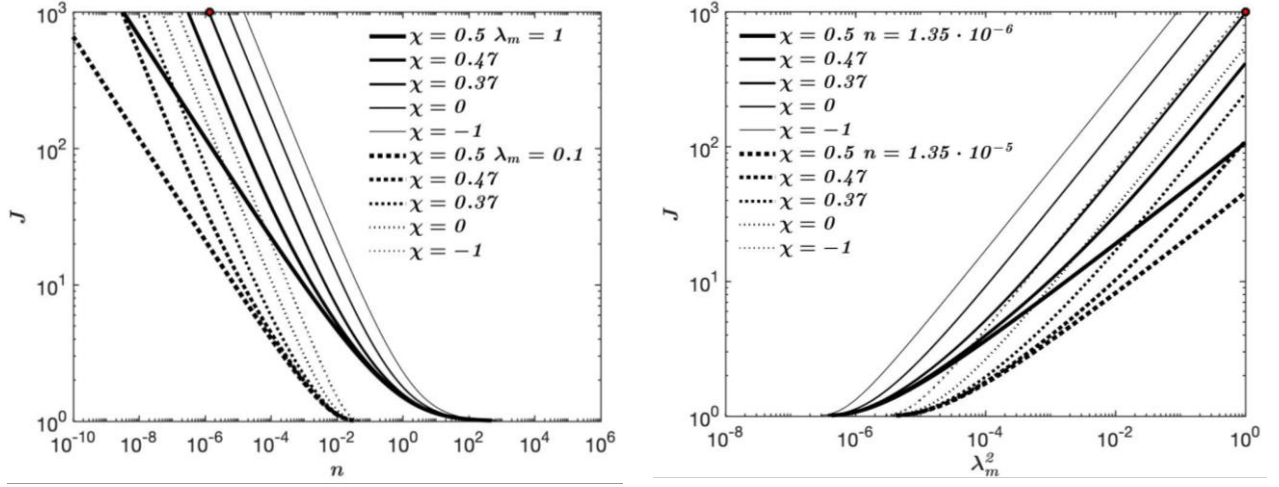


Figure 2 – Chemo-mechanical equilibrium conditions of a gel, given by $\bar{\mu} = 0$. *Left*: n versus J , from Eq. (26), at various χ and λ_m ; *Right*: λ_m^2 versus J , from Eq. (28), at various χ and n

Let us now define the free energy from Eq. (22). Figure 3 (left) plots $\bar{\psi}_e/n$ versus J and λ_m , and (right) $\bar{\psi}_m$ versus J and χ . These are taken from

$$\frac{\bar{\psi}_e}{n} = \frac{3}{2} \left(\frac{J^{2/3}}{\lambda_m^2} - 1 \right) - \ln J \quad (30a)$$

$$\bar{\psi}_m = (J - 1) \ln \left(1 - \frac{1}{J} \right) - \chi \left(1 - \frac{1}{J} \right) \quad (30b)$$

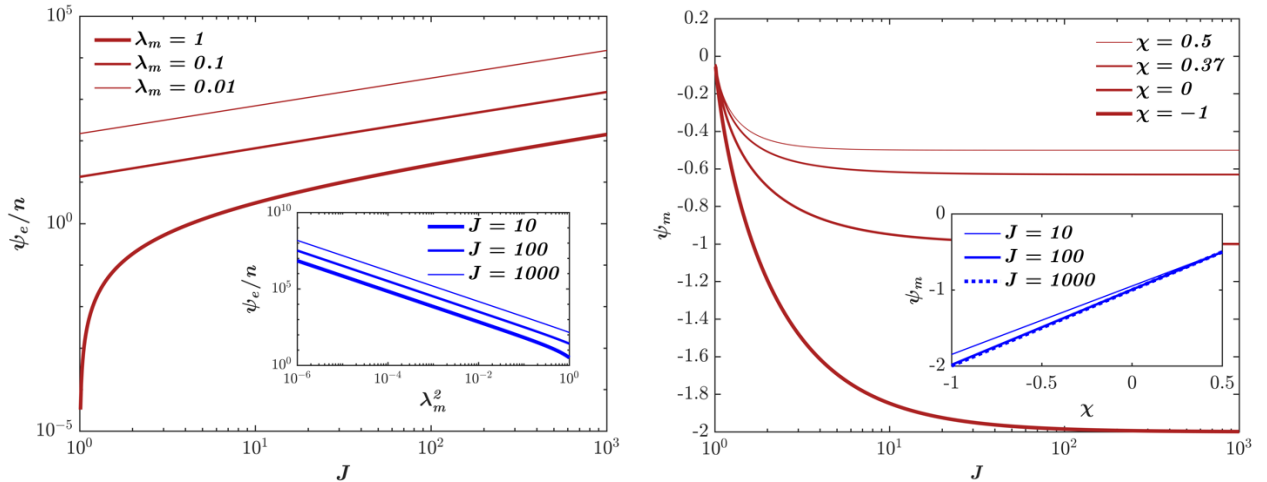


Figure 3 – *Left*: Dimensionless elastic free energy ratio $\bar{\psi}_e/n$ versus swelling ratio J and λ_m from Eq. (30a); *Right*: Dimensionless mixing energy $\bar{\psi}_m$ versus J and χ from Eq. (30b)

Figure 3 plots the relation expressed in Figure 3, with the normalized elastic free energy $\bar{\psi}_e/n$ on the left and the mixing free energy $\bar{\psi}_m$ on the right. The two components of free energy are inversely proportional during swelling.

In Figure 3-left, $\bar{\psi}_e/n$ increases with an increased swelling ratio J since the chains are stretched, thus decreasing the entropy of the system. Decreasing the chain microstretch λ_m leads to a greater $\bar{\psi}_e/n$, and here the difference between two red curves represents the injected energy in the fast motor (fm) activation case for CS-MM. The log-log plots in both the red curves and the blue curves in the inset of this figure show the linear trend $\bar{\psi}_e/n \sim 3J^{2/3}/2\lambda_m^2$ for larger J or smaller λ_m . This is due to the first term on the right-hand side of Eq. (30a).

In Figure 3-right, the mixing energy $\bar{\psi}_m$ decreases with increased J as more solvent is added to the mixture, thus increasing entropy. The semi-log plot in the red curves shows the asymptotic saturation energy $\bar{\psi}_{m,\infty} = -(1 + \chi)$ for large J . This also explains the linear correlation between $\bar{\psi}_m$ and χ in the blue curves in the inset.

The conditions $\chi = 0.37$, $J_0 = 1000$, $n_0 = 1.35 \cdot 10^{-6}$, and $\lambda_{m,0} = 1$, highlighted in Figure 2, in this case give $\bar{\psi}_{e,0}/n_0 = 1.42 \cdot 10^2$, $\bar{\psi}_{e,0} = 1.94 \cdot 10^{-4}$ and $\bar{\psi}_{m,0} = -0.63$. From this initial point, Figure 4 plots \bar{w}_{fm} and \bar{w}_{sm} as a function of the contraction ratio J_f/J_0 . In this figure, on the left we have CS-MM, *i.e.* by evolving λ_m at steady $n = n_0$, while on the right we have DC-MM, *i.e.* by evolving n at steady $\lambda_m = 1$. Both left and right plots show very similar results with slightly higher \bar{w}_{sm} for CS-MM than DC-MM for maximum contractions, *i.e.* lowest J_f/J_i , and larger n_0 . In this figure we can also observe that the work required to contract is proportional to the initial crosslink density n_0 and to the degree of contraction (high contraction giving low J_f/J_i). For $J_f/J_i \rightarrow 0$, we have that $\bar{w}_{sm}, \bar{w}_{fm} \rightarrow \infty$ (maximum contraction), while for $J_f/J_i = 1$ we have $\bar{w}_{sm}, \bar{w}_{fm} = 0$ (no contraction).

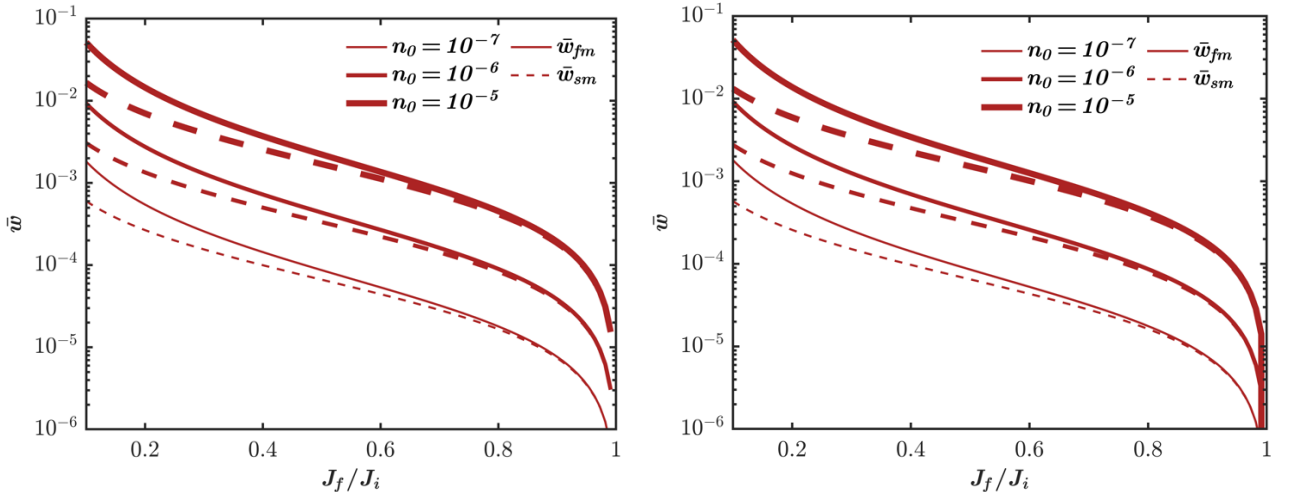


Figure 4 – *Left*: Dimensionless fast and slow motor work (\bar{w}_{fm} and \bar{w}_{sm}) versus contraction ratio J_f/J_0 for chain-shortening molecular motors (CS-MM); *Right*: Dimensionless fast and slow motor work (\bar{w}_{fm} and \bar{w}_{sm}) versus contraction ratio J_f/J_0 for dynamic crosslinking molecular motors (DC-MM).

Experimental comparison

The energetic requirement for contraction, predicted from our model, can be compared with experimental results from literature. Bendix et al. [18] conducted cytoskeletal gel contraction experiments observing the effects of chain density and motor concentration on contraction. They obtained that certain configurations yield observable contraction, while others yielded no observable contraction. Our model can explain this transition based on the required mechanical energy to allow contraction. The experiments consisted in varying crosslinker (α -actinin) and molecular motor (myosin II) concentrations, N_α and N_M respectively, with constant concentration of actin monomers, N_A . The gel specimens tested are of millimeter size, and the observable contractions were defined as achieving 90% volumetric deswelling ($J_f/J_i = 0.1$) in a timespan below 60 minutes. Given this long timescale of observation, related to specimen size, we consider contractile networks as those with sufficient concentration of MM so that they can exert the minimum work required for very slow contraction, *i.e.* w_{sm} . [18] reports the fixed concentration of actin monomers, as well as the ratios of myosin molecular motors $R_{M:A} = N_M/N_A$ and crosslinker α -actinin $R_{\alpha:A} = N_\alpha/N_A$ to actin. The crosslink (chain) density N relates to the crosslinker concentration N_α as $N = N_\alpha - N_b$ [22 ,23], giving

$$N = R_{\alpha:A}N_A - N_b \quad (31)$$

where N_b is the crosslinker density required to form the bundled network that then crosslinks. Eq. (31) assumes that, after bundling, each new crosslinking molecule splits an existing chain into two, therefore adding a new chain to the network.

We assume that the work provided by the MM scales with MM concentration as $w_{sm} = w_M N_M$, giving

$$w_{sm} = w_M R_{M:A} N_A \quad (32)$$

where w_M is the work provided by one MM. Eq (32) is based on the hypothesis of unlimited ATP availability and a that all motors equally contribute to provide a fixed mechanical work [24].

To determine the parameters of the gel at the 0 state, for each experimental value of $R_{\alpha:A}$, we estimate J_0 from the chemo-mechanical equilibrium in Eq. (26) with $\lambda_m = 1$ and $n_0 = N_0 \Omega$ from Eq. (31) ($N = N_0$). Here, N_A is extracted from the *current* density of actin monomers N_A/J_0 . Note that, χ is undefined, and we extract it from a test case in [18] as explained in Appendix C, where $J_0 = 1000$ and $n_0 = 1.35 \cdot 10^{-6}$, giving $\chi = 0.37$. The latter is material parameter, and thus is constant in each experiment.

To determine the parameters of the gel at the f state, we enforce again chemo-mechanical equilibrium from Eq. (26). From this equation, with $J_f = 0.1 J_0$ and χ , and we can extract $n = n_f$, under $\lambda_m = 1$ for DC-MM or λ_m from $n = n_0$ for CS-MM.

Finally, by substituting Eq. (30) into (25), we can calculate $\bar{w}_{sm} = w_{sm} \Omega / kT$. This result can then be substituted into Eq. (32) to extract the minimum required MM density N_M , based on the value of w_M . We adopt $w_M = 1.56 \cdot 10^{-14} J$ as a fitting parameter to compare our results in Figure 5. This value is equivalent to approximately 8 ATP molecules consumed per second, assuming a

constant contraction power for all the observed 60 minutes. This estimation is in qualitative agreement with the experimentally observed 3-5 ATP molecules per second [25].

Figure 5 shows a comparison between our estimated minimum MM density required to contraction (with red shading indicating non-contractile regions) with the observed contractile (black circles) and non-contractile (red crosses) conditions in [18]. Our estimation is shown in the bottom solid line for CS-MM, and dashed line for DC-MM. For most of the experimental data points, except some outliers, our estimation is validated. We speculate that the outlier data points are possibly due to incorrect contractile assay, where contractile gels could appear as non-contractile, or vice-versa, due to geometrical imperfections.

The upper bound to MM concentration in Figure 5 is due to a maximum strain energy per chain in the final state, $\psi_{e,f}/N_0$, above which the α -actinin crosslink breaks. In these conditions, contraction is prevented. As discussed in Appendix C, we adopt this energy maximum as $\psi_{e,f,max}/N_0 = 4.03 \cdot 10^{-17} J = 5800 kCal/mol$ ($1.59 \cdot 10^{-17} J = 2300 kCal/mol$) to fit the upper boundary of the contractile region for CS-MM (DC-MM). This value corresponds to the energy required to break one crosslink bond between the chains, and is equivalent to the energy of approximately 100 (50) hydrogen bonds.

In regions of high crosslinking, on the right side of Figure 5, contraction becomes much slower [17]. In the experimental timeframe of [18], contractions requiring more than 60 minutes were ignored, therefore classifying such trials as non-contractile. We speculate that the network associated with the red crosses on the right side of Figure 5 may still be contractile but requiring more than 60 minutes.

The contractile region predicted by our model is confirmed by experiments for the lower bound in Figure 5, highlighting the energetic limits of contraction in cytoskeletal networks. The upper bound motivated energetically by the structural limit of the actin backbone agrees well with experiments for CS-MM, while appears less accurate for DC-MM. This suggests that the proposed CS-MM model provides a more accurate energetic description of these gels.

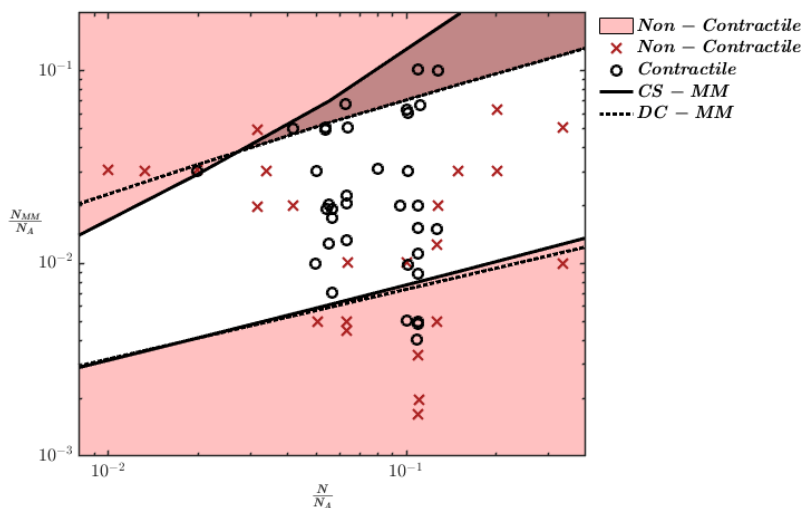


Figure 5 – Experimental comparison between number of molecular motors (N_{MM}) and chain density (N) during contraction. The bottom curves (lower bound) report the minimum N_{MM}

required for a volumetric contraction of 90%. The top curves (upper bound) report the maximum strain energy stored by an actin filament before rupture. Dashed lines present DC-MM while solid lines represent CS-MM.

It should finally be noted that our model considers the polymer backbone as composed of Gaussian (slack) chains. This hypothesis limits the reliability of our model, particularly in highly crosslinked networks (right side of Figure 5).

Conclusion

Contractile cytoskeletal networks exhibit a range of energetically motivated contractions caused by molecular motor activity. Our model introduces a more realistic molecular motor implementation, where chains shorten according to a ‘microstretch’ parameter. This approach yields similar results to that of previously employed chain density evolution models, particularly for highly swollen gels. Via simple steady state energetic analysis, under the simplest case of isotropic contraction, we quantify the mechanical energy required to achieve contraction as a function of polymer chain density and molecular motor density. We identify two limit cases, (*fm*) fast MM activation for which MM provide all the available mechanical energy immediately and (*sm*) slow MM activation where the timescale is much longer, and contraction is much slower. These two cases represent the maximum and minimum timescales for the contraction process. They also represent the two limits in the efficiency of energy transduction, where *sm* gives the highest efficiency and *fm* gives the lowest efficiency. This is because $w_{sm} < w < w_{fm}$, where w_{sm} provides the minimum energetic requirement for contraction, while w_{fm} provides the maximum energetic requirement. We observe that the energetic cost of contraction fulfilled by MM is proportional to chain density and MM density. Finally, we compare our results with experiments and observe good agreement, where the 90% contraction boundary is predicted by our model.

Our model provides an accurate and simple description of the energetic landscape of contraction for gels composed of slack chains. It also provides the minimum requirement of actin and myosin density to allow cytoskeletal contraction in such systems. Further development of this model will allow for a more comprehensive description of the cytoskeleton, *e.g.* composed of tight chains.

Acknowledgments

This work was supported by the New Frontiers in Research Funds – Exploration (NFRFE-2018-00730) and by the Natural Sciences and Engineering Research Council of Canada (NSERC) (RGPIN-2017-04464, and ALLRP554607-20).

Authors contributions

Conceptualization: M.F., M.B.; Execution: M.F., A.K., M.H., M.B.; Writing: M.F., A.K., G.J.E, D.A., M.B.

Appendix A

The first law of thermodynamics gives

$$\frac{d}{dt} \int_{V_d} e dV_d = \int_{S_d} T_j v_j dS_d + \int_{V_d} B_j v_j dV_d - \int_{S_d} N_j J_j^h dS_d - \int_{S_d} N_j h^q J_j^q dS_d \quad (\text{A1})$$

where e is the internal energy per unit reference volume, J_j^h is heat flux in the reference configuration, v_j is the velocity of elements in the volume and thus is the rate of change of x_j , h^q is the partial molar enthalpy of species q , B_j the body force vector, N_j the unit normal to boundary surfaces, and T_j the external traction force. Use of the divergence theorem and the principle of virtual power yields

$$\frac{de}{dt} = t_{jk} \frac{dF_{jk}}{dt} - \frac{\partial J_j^h}{\partial x_j} - \frac{\partial(h^q J_j^q)}{\partial x_j} \quad (\text{A2})$$

Entropy conservation is written as:

$$\frac{d}{dt} \int_{V_d} \eta dV_d = - \int_{S_d} N_j \frac{J_j^h}{T} dS_d - \int_{S_d} N_j \eta^q J_j^q dS_d + \int_{V_d} \dot{\eta}^p dV_d \quad (\text{A3})$$

where η is the entropy per unit volume in the reference state, η^k is the partial molar entropy of species k and $\dot{\eta}^p$ is the rate of entropy production per unit volume in the reference state. This leads to

$$\frac{d\eta}{dt} = - \frac{1}{T} \frac{\partial J_j^h}{\partial x_j} - J_j^h \frac{\partial}{\partial x_j} \left(\frac{1}{T} \right) - \frac{\partial(\eta^q J_j^q)}{\partial x_j} + \dot{\eta}^p \quad (\text{A4})$$

The Helmholtz energy per unit reference volume is

$$\psi = e - T\eta \quad (\text{A5})$$

The rate of change of the Helmholtz free energy is

$$\frac{d\psi}{dt} = t_{jk} \frac{dF_{jk}}{dt} - \frac{\partial(h^q J_j^q)}{\partial x_j} - \frac{J_j^h}{T} \frac{\partial T}{\partial x_j} + T \frac{\partial(\eta^q J_j^q)}{\partial x_j} - \eta \frac{dT}{dt} - T\dot{\eta}^p \quad (\text{A6})$$

Next, we introduce μ^q , the chemical potential of species q

$$\mu^q = h^q - T\eta^q \quad (\text{A7})$$

The rate of change of the specific Helmholtz energy, by taking the time derivative of (A5) and with species conservation is

$$\frac{d\psi}{dt} = t_{jk} \frac{dF_{jk}}{dt} - \left(\frac{\partial \mu^q}{\partial x_j} + \eta^q \frac{\partial T}{\partial x_j} \right) J_j^q - \frac{J_j^h}{T} \frac{\partial T}{\partial x_j} + \mu^q \left(\frac{dc^q}{dt} - Q_c^q \right) - \eta \frac{dT}{dt} - T\dot{\eta}^p \quad (\text{A8})$$

Assuming the Helmholtz free energy has a functional dependence described by (1), with (A8) we solve for the entropy production.

$$T\dot{\eta}^p = \left(t_{jk} - \frac{\partial\psi}{\partial F_{jk}} \right) \frac{dF_{jk}}{dt} + \left(\mu^q - \frac{\partial\psi}{\partial c^k} \right) \frac{dc^q}{dt} - \left(\eta + \frac{\partial\psi}{\partial T} \right) \frac{dT}{dt} - \left(\frac{\partial\mu^q}{\partial X_j} + \eta^k \frac{\partial T}{\partial X_j} \right) J_j^k - \frac{J_j^h}{T} \frac{\partial T}{\partial X_j} - \mu^q Q_c^q - \frac{\partial\psi}{\partial \zeta^j} \frac{d\zeta^p}{dt} \quad (\text{A9})$$

From the second law of thermodynamics, the rate of entropy production must be $\dot{\eta}^p \geq 0$. Considering chemical equilibrium, homogeneous and stationary distribution of temperature, and species conservation, which also implies no flux of species, and no change of cross-link density, the first 3 terms in parenthesis in (A9) are ≥ 0 for all deformation rates, concentration changes, and temperature adjustments whether positive or negative. This gives equations (3) and (4). With these satisfied, we are left with

$$- \left(\frac{\partial\mu^q}{\partial X_j} + \eta^q \frac{\partial T}{\partial X_j} \right) J_j^q - \frac{J_j^h}{T} \frac{\partial T}{\partial X_j} - \mu^q Q_c^q - \frac{\partial\psi}{\partial \zeta^p} \frac{d\zeta^p}{dt} \geq 0 \quad (\text{A10})$$

With the first term governing the transport of chemical species, the second term governing the flow of heat, and the third and fourth term together governing the flow of chemical reactions.

Appendix B

In this section we provide the mathematical derivation of the chain shortening contraction model strain energy. Gaussian chains are governed by the following end-to-end vector distribution

$$f(R_j) = \left(\frac{3}{2\pi\langle R^2 \rangle} \right)^{3/2} \exp\left(-\frac{3R^2}{2\langle R^2 \rangle} \right) \quad (\text{B1})$$

With $R_j = (X, Y, Z)$ the end-to-end vector of the chain and $R = \sqrt{X^2 + Y^2 + Z^2}$ the end-to-end length. Where X, Y, Z are the components of the end to end vector.

The mean of the squared end-to-end distance is given by

$$\langle R^2 \rangle = m_0 b^2 \quad (\text{B2})$$

Where m_0 is the average number of monomers in the chains, and b the average length of each segment in the chain. Gaussian chains are assumed to be non-interacting; their free energy is entirely entropic and governed by Boltzmann's entropy equation

$$g = -kT \ln(P(R_j)) \quad (\text{B3})$$

With the probability of finding a chain with a specific configuration given an end-to-end vector

$$P(R_j) = f(R_j) dX dY dZ \quad (\text{B4})$$

By applying stretches $\lambda_x, \lambda_y, \lambda_z$, a chain with ends initially occupying $dX dY dZ$ at R_j now occupies the volume $dx dy dz = \lambda_x dX \lambda_y dY \lambda_z dZ$ at $r_j = (x, y, z) = (\lambda_x X, \lambda_y Y, \lambda_z Z)$. The change in the free energy of the chain is therefore

$$\Delta g = kT \ln(P(R_j)/P(r_j)) \quad (\text{B5})$$

With

$$\frac{P(R_j)}{P(r_j)} = \frac{f(R_j)}{f(r_j)} \frac{1}{\lambda_x \lambda_y \lambda_z} = \left(\frac{\langle r^2 \rangle}{\langle R^2 \rangle} \right)^{3/2} \exp\left(\frac{3}{2} \left(\frac{r^2}{\langle r^2 \rangle} - \frac{R^2}{\langle R^2 \rangle} \right) \right) \frac{1}{\lambda_x \lambda_y \lambda_z} \quad (\text{B6})$$

And therefore

$$\Delta g = \frac{3kT}{2} \left(\left(\frac{\lambda_x^2}{\langle r^2 \rangle} - \frac{1}{\langle R^2 \rangle} \right) X^2 + \left(\frac{\lambda_y^2}{\langle r^2 \rangle} - \frac{1}{\langle R^2 \rangle} \right) Y^2 + \left(\frac{\lambda_z^2}{\langle r^2 \rangle} - \frac{1}{\langle R^2 \rangle} \right) Z^2 + \ln \frac{\langle r^2 \rangle}{\langle R^2 \rangle} \right) - kT \ln(J) \quad (\text{B7})$$

A network of Gaussian chains is constructed by summing the free energies of \bar{N} individual chains. Furthermore, we assume that the ends of each chain are terminated by crosslinks which deform affinely with the network. The free energy density of a network of Gaussian chains is therefore

$$\begin{aligned} \psi_e &= \frac{1}{V_0} \sum_{i=1}^{\bar{N}} \Delta g_i \\ &= \frac{1}{V_0} \sum_{i=1}^{\bar{N}} \left(\frac{3kT}{2} \left(\left(\frac{\lambda_x^2}{\langle r^2 \rangle} - \frac{1}{\langle R^2 \rangle} \right) X^2 + \left(\frac{\lambda_y^2}{\langle r^2 \rangle} - \frac{1}{\langle R^2 \rangle} \right) Y^2 + \left(\frac{\lambda_z^2}{\langle r^2 \rangle} - \frac{1}{\langle R^2 \rangle} \right) Z^2 + \ln \frac{\langle r^2 \rangle}{\langle R^2 \rangle} \right) - kT \ln(J) \right) \end{aligned} \quad (\text{B8})$$

With sufficiently many chains we may rewrite (B8) as

$$\psi_e = \frac{3NkT}{2} \left(\left(\frac{\lambda_x^2}{\langle r^2 \rangle} - \frac{1}{\langle R^2 \rangle} \right) \langle X^2 \rangle + \left(\frac{\lambda_y^2}{\langle r^2 \rangle} - \frac{1}{\langle R^2 \rangle} \right) \langle Y^2 \rangle + \left(\frac{\lambda_z^2}{\langle r^2 \rangle} - \frac{1}{\langle R^2 \rangle} \right) \langle Z^2 \rangle + \ln \frac{\langle r^2 \rangle}{\langle R^2 \rangle} \right) - NkT \ln(J) \quad (\text{B9})$$

where we defined the chain density $N = \bar{N}/V_0$ as well as the expected squared values for the coordinates of the end-to-end vector of a chain $\langle X^2 \rangle, \langle Y^2 \rangle, \langle Z^2 \rangle$. These are typically related to the expected end-to-end distance squared by virtue of symmetry in the three coordinate directions.

$$\langle X^2 \rangle = \langle Y^2 \rangle = \langle Z^2 \rangle = \frac{\langle R^2 \rangle}{3} = \frac{m_0 b^2}{3} \quad (\text{B10})$$

Additionally, we have $\langle r^2 \rangle = \langle R^2 \rangle$, because the deformation, chain length and number of monomers are all constant. However, in the presence of chain shortening molecular motors, the average number of links in a chain may decrease to $m < m_0$ and the statistical distribution of chains deviate from that described in (B1). If we define a microstretch parameter $\lambda_m^2 = m/m_0 = \langle r^2 \rangle / \langle R^2 \rangle$, we ultimately find

$$\psi_e = \frac{3NkT}{2} \left(\left(\frac{\lambda_x^2}{\lambda_m^2} - 1 \right) \frac{1}{3} + \left(\frac{\lambda_y^2}{\lambda_m^2} - 1 \right) \frac{1}{3} + \left(\frac{\lambda_z^2}{\lambda_m^2} - 1 \right) \frac{1}{3} + \frac{3}{3} \ln \lambda_m^2 \right) - NkT \ln(J) \quad (\text{B11a})$$

$$\psi_e = \frac{NkT}{2} \left(\left(\frac{\lambda_x^2}{\lambda_m^2} - 1 \right) + \left(\frac{\lambda_y^2}{\lambda_m^2} - 1 \right) + \left(\frac{\lambda_z^2}{\lambda_m^2} - 1 \right) + 2 \ln \lambda_m^3 - 2 \ln(J) \right) \quad (\text{B11b})$$

$$\psi_e = \frac{NkT}{2} \left(\frac{\lambda_x^2 + \lambda_y^2 + \lambda_z^2}{\lambda_m^2} - 3 - 2 \ln \left(\frac{J}{\lambda_m^3} \right) \right) \quad (\text{B11c})$$

Which is the free energy of a network of Gaussian chains subjected to macroscopic stretching $\lambda_x^2 + \lambda_y^2 + \lambda_z^2 = F_{jk} F_{jk}$ in the coordinate axes and microscopic evolution in the form of chain shortening.

Appendix C

We determine the model parameters based on data from a specific contraction experiment performed by Bendix et al. [18] with data provided in the supplementary materials. We know the

actin bundle (chain) density in the swollen state to be $N_{i,i} = 4.78 \cdot 10^{17} m^{-3}$ based on Eq. 27, with $R_{\alpha:A} = 0.11$, with $C_A = 2.38 \cdot 10^{-5} M$ and $N_b = 1.43 \cdot 10^{21} m^{-3}$. N_b is derived from the number of crosslinks needed to form a single bundle, which is based on bundles of $1.5 \mu m$ [18] diameter with chains of diameter $5 nm$ [26]. Two linked actin chains take up approximately $50 nm$ due to α -actinin crosslinker spacing [27]. Since actin chains are $5 \mu m$ [18] long and made up of $5 nm$ [26] monomers, given the total concentration of actin monomers C_A we can derive the crosslinkers required to form one bundle ($1.25 \cdot 10^3$) given we link every 10 monomers [27]. We calculate the un-crosslinked bundle density to be $4.78 \cdot 10^{17} m^{-3}$, requiring α -actinin density of $1.43 \cdot 10^{21} m^{-3}$ to assemble. Given the concentration of α -actinin is $C_\alpha = 2.6 \cdot 10^{-6} M$ there remain $1.43 \cdot 10^{20} m^{-3}$ crosslinkers. This is the chain density in the swollen state: $\hat{N}_0 = 1.43 \cdot 10^{20} m^{-3}$. The swollen volume $V_0 = 0.88 \mu L$ [18] and assuming cylindrical chains of diameter $5 nm$ the dry volume is $V_d = 0.001 \mu L$. This yields an initial swelling ratio of $J_0 = J_i = 880 \approx 1000$. Therefore, $N_0 = J_0 \hat{N}_0 = 5.09 \cdot 10^{22} m^{-3}$ and $n_0 = N_0 \Omega = 1.35 \cdot 10^{-6}$.

The motor work was determined to be $w_{MM} = 1.56 \cdot 10^{-14} J$. This is equivalent to burning approximately 10 ATP/sec for a contraction lasting 1 hour as in the experimental timeframe [18]. In the case of DC MM $w_{MM} = 1.36 \cdot 10^{-14} J$

The maximum strain energy per chain boundary is achieved with $\psi_{e,f,max}/N_0 = 4.03 \cdot 10^{-17} J = 5800 kCal/mol$ in the case of CS-MM and $\psi_{e,f,max}/N_0 = 1.59 \cdot 10^{-17} J = 2300 kCal/mol$ for DC-MM.

Other constants used in graphing and experimental comparisons, $\Omega = 3 \cdot 10^{-30} m^3$, $kT = 4.14 \cdot 10^{-21} J$, $\chi = 0.3667$.

References

- [1] Boal, D.H. (2002) Mechanics of the cell. *Cambridge University Press*.
- [2] Bertrand, O.J.N., Fygenson, D.K., and Saleh, O.A. (2012) Active, motor-driven mechanics in a DNA gel. *Proceedings of the National Academy of Sciences of the United States of America*. 109 (43), 17342–17347.
- [3] Gardel, M. L., Shin J. H., MacKintosh F. C., Mahadevan L., Matsudaira P., Weitz D. A. (2004) Elastic Behavior of Cross-Linked and Bundled Actin Networks. *Science*, 304(5675), 1301–1305.
- [4] Mackintosh, F.C. and Levine, A.J. (2008) Nonequilibrium mechanics and dynamics of motor-activated gels. *Physical Review Letters*. 100 (1).
- [5] Kruse, K., Joanny, J.F., Jülicher, F., Prost, J., and Sekimoto, K. (2005) Generic theory of active polar gels: A paradigm for cytoskeletal dynamics. *European Physical Journal E*. 16 (1), 5–16.
- [6] Hong, W., Zhao, X., Zhou, J., and Suo, Z. (2008) A theory of coupled diffusion and large deformation in polymeric gels. *Journal of the Mechanics and Physics of Solids*. 56 (5), 1779–1793.
- [7] Bacca, M., Saleh, O.A., and Mcmeeking, R.M. (2019) Contraction of polymer gels created by the activity of molecular motors. *Soft Matter*. 12(15), 4467–4475.
- [8] Curatolo, M., Nardinocchi, P., and Teresi, L. (2020) Dynamics of active swelling in contractile polymer gels. *Journal of the Mechanics and Physics of Solids*. 135.
- [9] Doi, M. (2009) Gel dynamics. *Journal of the Physical Society of Japan*. 78 (5).

- [10] Rossi, M., Nardinocchi, P., and Wallmersperger, T. (2019) Swelling and shrinking in prestressed polymer gels: An incremental stress-diffusion analysis. *Proceedings of the Royal Society A: Mathematical, Physical and Engineering Sciences*. 475 (2230).
- [11] Mazaheri, H., Baghani, M., and Naghdabadi, R. (2016) Inhomogeneous and homogeneous swelling behavior of temperature-sensitive poly-(N-isopropylacrylamide) hydrogels. *Journal of Intelligent Material Systems and Structures*. 27 (3), 324–336.
- [12] Hong, W., Zhao, X., Zhou, J., and Suo, Z. (2008) A theory of coupled diffusion and large deformation in polymeric gels. *Journal of the Mechanics and Physics of Solids*. 56 (5), 1779–1793.
- [13] Koenderink, G.H., Dogic, Z., Nakamura, F., Bendix, P.M., Mackintosh, F.C., Hartwig, J.H., et al. (2009) An Active Biopolymer Network Controlled by Molecular Motors. *PNAS*. 106(36) 15192-15197.
- [14] Alvarado, J., Sheinman, M., Sharma, A., MacKintosh, F.C., and Koenderink, G.H. (2017) Force percolation of contractile active gels. *Soft Matter*. 13 (34), 5624–5644.
- [15] Curatolo, M., Nardinocchi, P., and Teresi, L. (2021) Mechanics of active gel spheres under bulk contraction. *International Journal of Mechanical Sciences*. 193.
- [16] Rossi, M., Nardinocchi, P., and Wallmersperger, T. (2019) Swelling and shrinking in prestressed polymer gels: An incremental stress-diffusion analysis. *Proceedings of the Royal Society A: Mathematical, Physical and Engineering Sciences*. 475 (2230).
- [17] Janson, L.W., Kolega, J., and Lansing Taylor, D. (1991) Modulation of Contraction by Gelation/Solution in a Reconstituted Motile Model.
- [18] Bendix, P.M., Koenderink, G.H., Cuvelier, D., Dogic, Z., Koeleman, B.N., Briehar, W.M., et al. (2008) A quantitative analysis of contractility in active cytoskeletal protein networks. *Biophysical Journal*. 94 (8), 3126–3136.
- [19] Miyata, H., Yasuda, R., & Kinosita, K. (1996). Strength and lifetime of the bond between actin and skeletal muscle alpha-actinin studied with an optical trapping technique. *Biochimica et Biophysica Acta*, 1290, 83–88.
- [20] Ferrer, J. M., Lee, H., Chen, J., Pelz, B., Nakamura, F., Kamm, R. D., & Lang, M. J. (2008). Measuring molecular rupture forces between single actin filaments and actin-binding proteins. *PNAS* 105(27).
- [21] Flory, P.J. and Rehner, J. (1943) Statistical mechanics of cross-linked polymer networks II. Swelling. *The Journal of Chemical Physics*. 11 (11), 521–526.
- [22] Falzone, T.T., Lenz, M., Kovar, D.R., and Gardel, M.L. (2012) Assembly kinetics determine the architecture of α -actinin crosslinked F-actin networks. *Nature Communications*. 3.
- [23] Wachsstock, D.H., Schwarz, W.H., and Pollard, T.D. (1993) Affinity of α -Actinin for Actin Determines the Structure and Mechanical Properties of Actin Filament Gels.
- [24] Kane, R.E. (1983) Interconversion of Structural and Contractile Actin Gels by Insertion of Myosin During Assembly. *J Cell Biol*. 97(6), 1745-1752.
- [25] Zhen H., Bottinelli R., Pellegrino M. A., Ferenczi M. A., Reggiani C. (2000) ATP Consumption and Efficiency of Human Single Muscle Fibers with Different Myosin Isoform Composition. *Biophysical Journal*. 79(2), 945–961.
- [26] Ron M., Phillips R., Orme N. (2015) Cell Biology by the Numbers.
- [27] Winkelman, J.D., Suarez, C., Hocky, G.M., Harker, A.J., Morganthaler, A.N., Christensen, J.R., et al. (2016) Fascin and α -Actinin Bundled Networks Contain Intrinsic Structural Features that Drive Protein Sorting. *Current Biology*. 26 (20), 2697–2706.